MANNGA Deliverable

D2.2 List and description of fabricated and characterised 2D freestanding YIG CMRs on LPE YIG media, including their measured KPIs.

Version 1.0

Grant Agreement number	101070347
Action Acronym	MANNGA
Action Title	MAGNONIC ARTIFICIAL NEURAL NETWORKS AND GATE ARRAYS
Call	HORIZON-CL4-2021-DIGITAL-EMERGING-01
Version date of the Annex I against which the assessment will be made	31.5.2022
Start date of the project	1.9.2022
Due date of the deliverable	31.8.2023
Actual date of submission	13.10.2023
Lead BEN / AP for the deliverable	Martin-Luther-Universität Halle-Wittenberg (MLU)
Dissemination level of the deliverable	Public

Action Coordinator, PI
Sebastiaan van Dijken
AALTO KORKEAKOULUSÄÄTIÖ SR, Aalto University School of Science

Action Scientific coordinator
Volodymyr Kruglyak
THE UNIVERSITY OF EXETER

Co-funded by the European Union

MANNGA project is partly funded by the European Union. Views and opinions expressed are however those of the author(s) only and do not necessarily reflect those of the European Union or HADEA. Neither the European Union nor the granting authority can be held responsible for them.

Authors in alphabetical order		
Name	Beneficiary	e-mail
Georg Schmidt	MLU	Georg.schmidt@physik.uni-halle.de
Rouven Dreyer	MLU	Rouven.dreyer@physik.uni-halle.de

Document reviewers		
Name	Beneficiary	e-mail
Volodymyr Kruglyak	UNEXE	V.V.Kruglyak@exeter.ac.uk
Andrey Shytov	UNEXE	a.shytov@exeter.ac.uk
Sebastiaan van Dijken	AALTO	Sebastiaan.van.dijken@aalto.fi

Abstract

All-YIG CMR structures were fabricated in Halle. After initial discussions, it was decided to start with a process using a non-magnetic interlayer between two YIG films. First large area samples were fabricated and showed a suitable damping. These results were used for the realization of 12 CMR structures, a number of which were characterized by scanning TR-MOKE. Little effect was observed so far, and further optimization will follow based on optimized process steps, with insights from theory and taking into account the inhomogeneous broadening of the YIG on AlOx.

Contents

1. Fabrication of all-YIG CMRs

This deliverable describes the fabrication and characterization of the project's first functional all-yttrium-iron-garnet (all-YIG) chiral magnonic resonator (CMR) structures. First, a new technology for the all-YIG CMR fabrication is introduced and then the first results on optical characterization are shown.

Figure 1.1 shows a schematic of an all-YIG CMR structure, with the dimensions corresponding to the structures in-depth described in this deliverable.

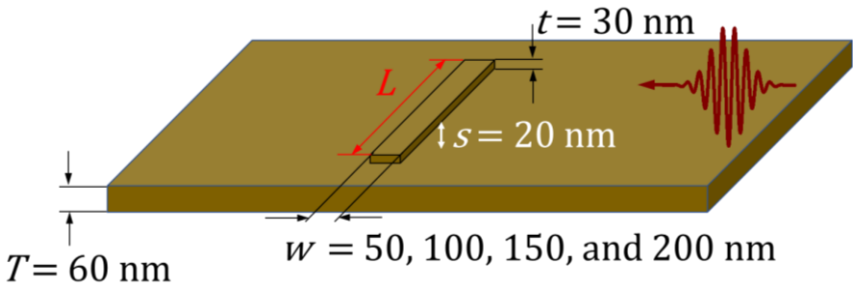

Fig. 1.1. Schematic drawing of the fabricated structures forming the all-YIG CMRs. The bottom large area film of YIG grown by liquid-phase epitaxy (LPE) can also be patterned into a stripe waveguide, while the spacing between top and bottom YIG films can be realized either by air and a free-standing part at the top or by a non-magnetic interlayer.

As Fig. 1.1 shows, there is a constant spacing required between the bottom layer and the YIG stripe on top. Two different strategies were discussed. The first plan was to make the top YIG film as a free-standing 'bridge'. It is, however, difficult to define an exact and constant spacing between the YIG bridge and the bottom YIG film for large values of the bridge length L. Therefore, a second alternative was evaluated and optimized in parallel. For the demonstrator CMR devices, an ultralow damping in the bridge is not required. So, we have grown YIG bridges on an GGG substrate with an AlOx spacer layer at room temperature. After annealing, the YIG is polycrystalline; however, its damping is still in a range acceptable for demonstration of the CMR functionalities, according to the theoretical modelling performed at the UNEXE team.

Figure 1.2 shows results of experimental characterisation of the polycrystalline YIG thin-film material of the bridge part of the CMRs performed using the frequency dependent ferromagnetic resonance (FMR) measurements.

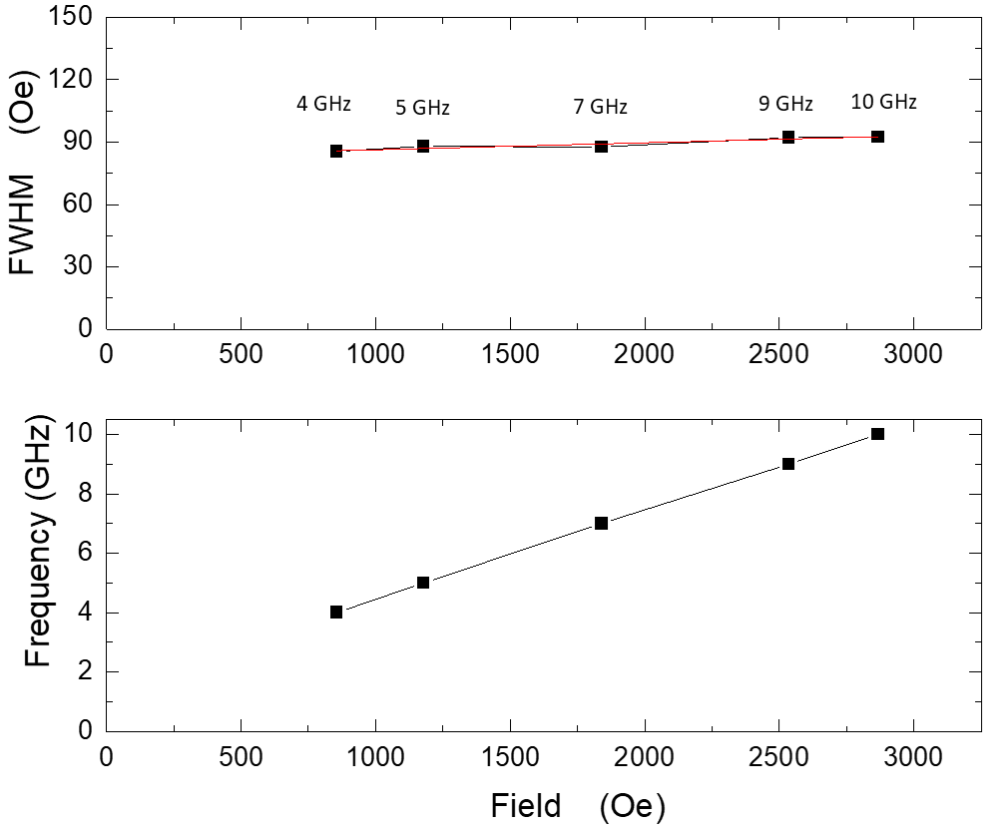

Fig. 1.2. FMR measurements for a 100 nm thick YIG film grown on an AlOx interlayer. The bottom panel shows the dependence of the resonance frequency on the bias magnetic field. The top panel shows the dependence of the resonance linewidth (as full width at half maximum, FWHM) on the bias field. The fit indicates the Gilbert damping value of $\alpha \approx 1.5 \times 10^{-3}$.

The results of the FMR measurements of the polycrystalline YIG material indicate a damping in the range of $\alpha \approx 1.5 \times 10^{-3}$, which is at the level of best (in terms of the damping) ferromagnetic metals. The samples, however, show a substantial inhomogeneous broadening. It is to be expected that this broadening is due to the polycrystalline nature of the material and appears due to a distribution in the orientations of grains and grain boundaries. For a nanostructure, however, we may expect much less broadening.

Based on these results, we have fabricated a total of 12 CMR structures. For the bottom layer we used 60 nm thick LPE-grown films fabricated by INNOVENT. On top of these films, the YIG CMR stripes and markers were defined by electron beam lithography. Subsequently 20 nm of AlOx were deposited by e-gun evaporation followed by 30 nm of YIG deposited by PLD at room temperature. After annealing, metal microwave antennae were fabricated by e-beam lithography, metal evaporation (Ti/Au) and lift-off.

Figure 1.3 shows an overview of a sample with three CMR structures of different stripe width.

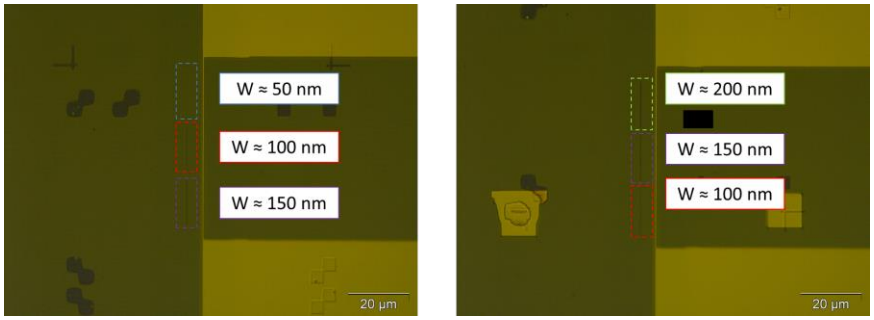

Fig. 1.3. Optical microscopy image of two different samples showing the gold antenna and three AlOx/YIG stripe with different respective width.

Detailed analysis was also done by scanning electron microscopy. As Fig. 1.4 shows, there is an asymmetry in the lines that needed further investigation. Elemental analysis by EDX in the electron microscopes indicates that the lateral broadening is due to the AlOx and the YIG stripes should still be homogeneous.

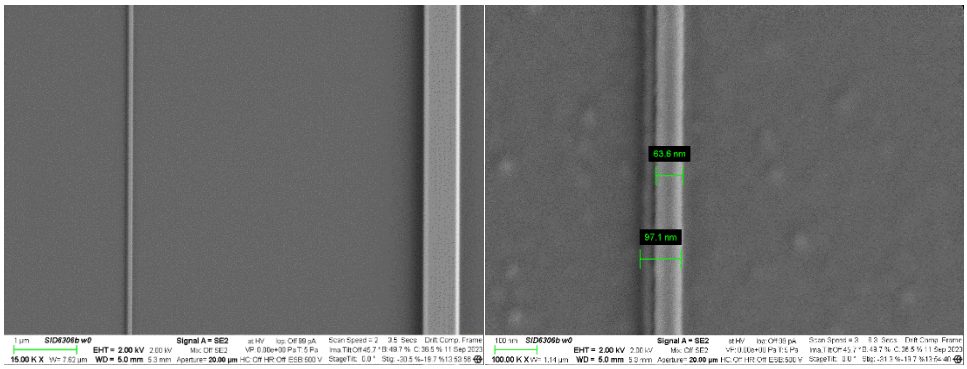

Fig. 1.4.: Left hand side: SEM image of a AlOx/YIG stripe and the corresponding RF antenna. Right hand side: zoom in showing that the width slightly deviates and that on the left hand side, one of the two layers is broadened. As EDX shows this part is AlOx.

In the next generation of devices this asymmetry will be taken care of by separating the lithography steps for the AlOx and the YIG lift-off, making the AlOx stripe much wider than the YIG one.
After finishing the fabrication samples were diced and forwarded for characterization. In a next step, we also plan to analyse the crystallinity of the stripes by transmission electron microscopy at Aalto using target preparation by focused ion beam.

2. Optical detection of spin waves in YIG-based CMRs

In our part of the MANNGA project, we focus on YIG-based CMRs fabricated in HALLE in order to investigate how the properties of these all YIG CMR structures differ from hybrid metal-YIG CMR devices. In the last year, we have optimized the Super-Nyquist-Sampling MOKE (SNS-MOKE) setup in

our lab in terms of detection sensitivity which allows us to precisely detect linear and non-linear excitations of spin waves.

We performed initial characterization steps on a sample with four different CMR geometries. This width of the CMRs varies between 50 nm and 200 nm while the thickness was kept constant at 30 nm. The experimental configuration was as follows. The external bias magnetic field was applied in the direction of the CMR structure corresponding to the Damon-Eshbach (DE) geometry. The field amplitude was set either to +/- 3 mT or +/- 5 mT. In this geometry, we detected the dynamic response locally behind the CMR structure while the excitation frequency was swept.

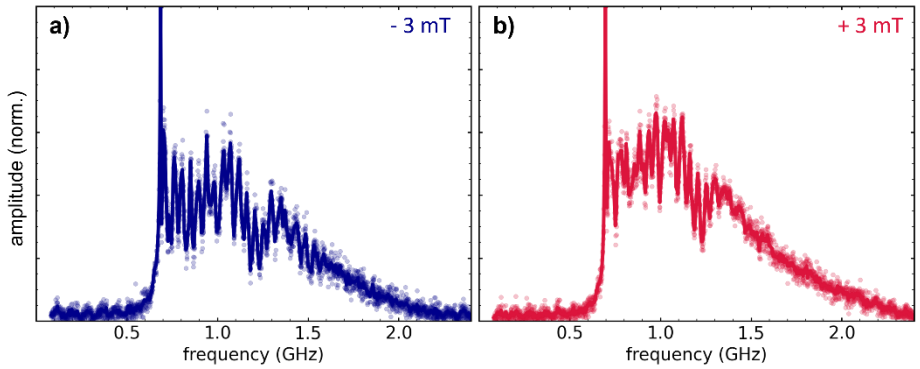

Fig 2.1. The normalized spin wave amplitude measured locally behind the CMR structure with a width of 150 nm for negative field in a) and positive field direction in b).

In the first set of measurements no clear band gap was visible for the different in plane field directions for the 150 nm wide YIG CMR. However, the band gap expected from simulations carried out in UNEXE for this specific type of CMR structure (with somewhat different dimensions) is supposed to be small, and thus, the measurements need to be carried in much finer steps. These measurements are currently under way, considering different bias fields, rf-frequencies as well as rf-driving powers.

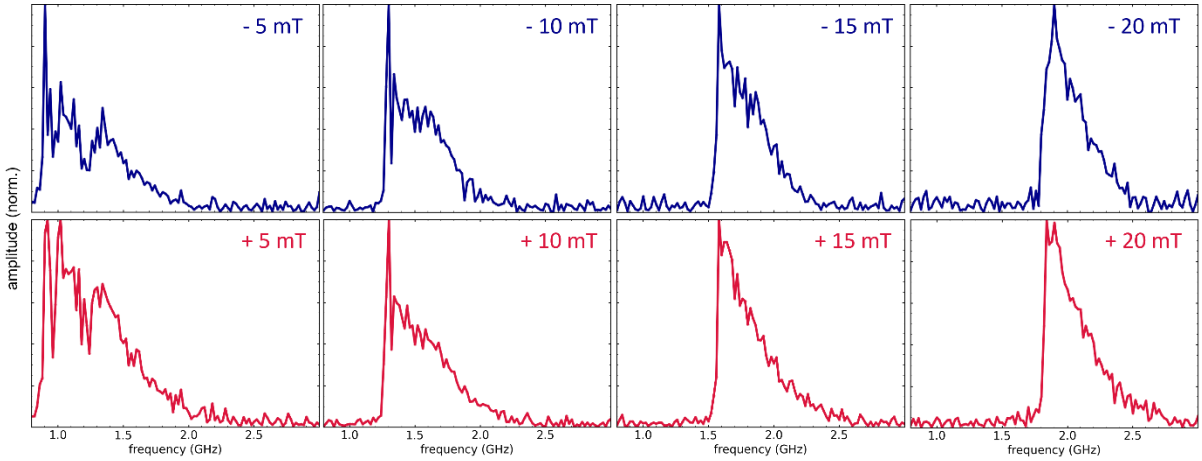

Fig 2.2. Normalized spin-wave spectra for different external bias fields. Only in the low field regime (+/-5 mT) clear changes between the two field directions become visible.

In a second step, we performed similar measurements for different values of the external bias field in order to confirm the theoretically obtained field regime in which these CMRs should be operated. As shown in Fig. 2.2., we can clearly see a strong change of the obtained spectra for different field directions at low bias field values (+/- 5 mT). For larger fields the spectra appear to be more similar, indicating no chirality dependent effect at this field amplitudes.

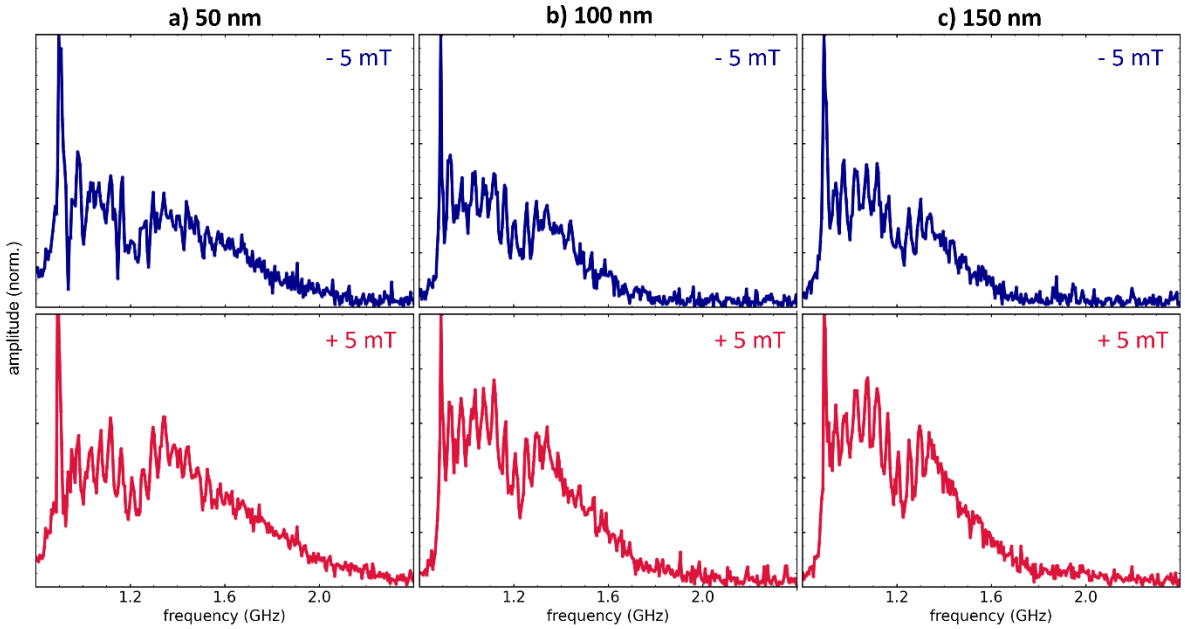

Fig 2.3. Spin wave spectra for different field orientations are shown for CMR widths of a) 50 nm, b) 100 nm and c) 150 mn. Measurements where obtained roughly 3 µm behind the CMRs.

As a next step, we tried to find changes in such spectra induced by the width of the CMR. As shown in Fig 2.3, it appears that the 50 nm structure in Fig 2.3 a) shows a slightly different spin wave propagation for positive field direction compared to the ones in b) and c). So far, spatially resolved imaging for a set of two different field amplitudes and rf-frequencies has been carried out for the 150 nm structure. In contrast to hybrid metal-YIG CMRs, no clear indication of a chirality dependent phase shift is observed in these measurements between +5 mT and -5 mT for the frequency values investigated.

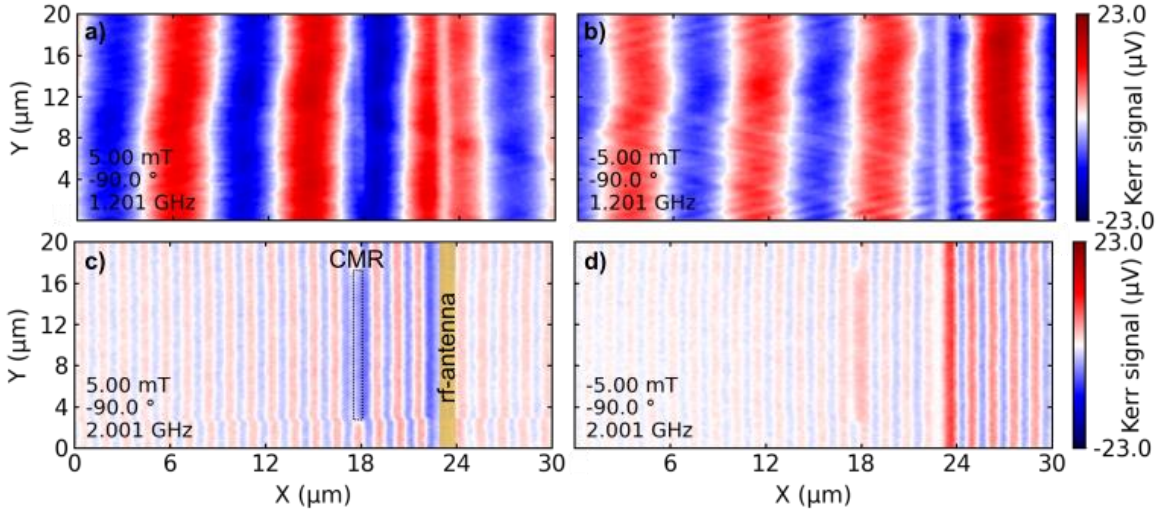

Fig 2.4. Spatially resolved imaging of the 150 nm structure for excitation frequencies of 1.2 GHz and 2 GHz, each for two different field orientations. The rf-antenna is located at around 24 μm while the CMR is at 18 μm.

Additional recent simulations were carried out at UNEXE for the structures presented here. The key conclusions from the modelling are as follows.

- For 50 nm- and 100 nm-wide CMRs, the resonant frequencies are above 2 GHz and are apparently outside the spectrum of incident spin waves. Detecting such resonances could prove challenging.
- For w=150nm, the resonant frequencies move below 2 GHz.
- The resonant frequency and its strength are quite sensitive to whether the resonator is magnetised parallel or antiparallel to the film. In the antiparallel configuration, the resonant frequency is noticeably lower. However, the signatures of such a resonance in the transmitted amplitude are rather weak, e.g. the amplitude is reduced by mere 10%. The effect in phase is much stronger, and there is a strong asymmetry between the forward and backward directions. To observe it experimentally, one needs to be quite close to the resonance.

In Fig 2.4 (data from 150 nm-wide CMR), the only aspect resembling what was observed for hybrid metal-YIG CMRs is the appearance of caustic features for 1.2 GHz at -5 mT in Fig 2.4b), which are absent in at +5 mT panel a). In addition, we observe a visible interaction of the propagating spin wave with the CMR in c) and d), indicating a quasi-uniform precessional mode within the CMR. For these device structures, further measurements under different conditions are planned in order to experimentally demonstrate the predicted behaviour and precisely map the parameter space for their functionality.